# Chapter 9
## The Results of the Integrated Design

*"An important scientific innovation rarely makes its way by gradually winning over and converting its opponents: it rarely happens that Saul becomes Paul. What does happen is that its opponents gradually die out and that the growing generation is familiarized with the idea from the beginning." -- Max Planck*

This chapter presents the results of experiments conducted in the Virginia Tech supersonic wind tunnel on a newly designed integrated fuel injection/ignition system, consisting of a four-holed aeroramp and a plasma torch. The plasma torch is a low-power design, capable of operating on various hydrocarbon and inert feedstocks from 0.5-4.5 kW. The aeroramp injector consists of four flush-wall holes, oriented to produce vortical motions ideal for mixing. In the present experiments, methane, ethylene, nitrogen, and air feedstocks were fed through the torch, while air and ethylene were forced through the injector. The main scope of the work was to determine how the lifting effect of the aeroramp affected the plasma jet, and to ascertain how the injection of fuel through the aeroramp and the power supplied to the torch affected the radical distributions downstream of the plasma jet. The aeroramp was observed to have a strong lifting effect on the plasma jet, especially for injector momentum flux ratios above 1.5. In addition, the amount of power supplied to the torch produced an exponential effect on the emission intensity of the radicals observed downstream of the plasma jet. This exponential increase in emission is a result of an increased fuel-plasma interaction rate.

In order to develop a practical scramjet combustor, careful consideration must be given to the integration of various components within the combustor, particularly the fuel injection and ignition systems. The design of any supersonic combustor must balance the mixing and combustion characteristics that are desired with the necessary total pressure losses induced to achieve such conditions. Successful ignition and flameholding by the use of a plasma torch in a supersonic cross flow has been well documented in the literature review. In addition, the enhanced mixing provided by aeroramp injectors using carefully arranged injection orifices to produce streamwise vortices have also been shown. The experiments presented here were designed to investigate the combination of an aeroramp injector with a plasma torch, and to search for possible synergistic effects of

the combination. The design and development of the aeroramp is reported by Jacobsen (2001), while the plasma torch design is presented in Chapter 2. In addition, Jacobsen reports on investigations of the torch placement relative to the fuel injector, which is not covered here. The goals of the research were to discover the extent to which the aeroramp provided a lifting effect to the plasma jet, and determine the trends associated with the emission intensity of downstream through changes in the torch power and injector fuel flowrate. Methane, ethylene, nitrogen, and air were used as torch feedstocks to determine the effects of using excited hydrocarbon, nitrogen, and oxygen species to interact with the ethylene fed through the injector. In preliminary experiments, air was fed through the injector in place of ethylene to study the lifting effect of the aeroramp. Further experiments with the integrated design fed ethylene through the injector to determine how the injector fuel flowrate and torch power affected the amount of fuel-plasma interaction.

To evaluate the performance of a particular test configuration, spectrographic methods, filtered photography, and total temperature sampling were used. These methods were designed to support one another in creating a clearer overall picture of the phenomena associated with such a device. Filtered photography was used to look at the local phenomena surrounding the jet, whereas spectrographic methods were used to measure the distribution of species just downstream of the jet. Total temperature measurements provided a far-downstream look at how the thermal energy from the torch was mixed into the aeroramp plumes.

Spectrographic evaluation was made through the use of a CCD-spectrometer and positioning devices, so that the radical distributions downstream of the torch could be mapped while the torch was in operation. One difficulty associated with the spectrographic measurements occurred when ethylene was fed through the injector and methane was fed through the torch. Under these circumstances it was difficult, if not impossible, to determine which emitting hydrocarbon species were associated with which source. In addition, spectral measurements of the plasma and downstream regions showed little evidence of the OH radical, indicating that only a small fraction of fuel was undergoing combustion. Therefore, noting these difficulties, the emission observed for the methane-ethylene experiments will be reported as a result of the combined effect of

fuel dissociation, any type of chemical reaction occurring between the plasma and fuel, and combustion, however limited its contribution might be.

To study the lifting effect of the aeroramp injector, air, rather than fuel, was fed through the injector so that the radicals produced by the methane plasma torch could be easily tracked without the injector acting as a second hydrocarbon source as described above. Studies of the lifting effect created by the aeroramp showed that the aeroramp had a profound effect on the penetration height of the plasma jet, particularly for injector momentum flux ratios above 1.5. Conversely, the power of the torch was observed to have very little effect on the penetration height of the plasma jet, except for powers above 3000 W where the plasma jet experiences a slight increase in penetration height. Spectrographic evaluation of the radical distributions downstream of the plasma jet showed that increasing torch power had an exponential effect on the emission intensity of plasma-fuel products, regardless of the amount of fuel fed through the injector. In addition, due to the unheated tunnel conditions, increasing the fuel flowrate through the injector was observed to decrease the emission intensity. This was attributed to the fuel acting as a heat sink. Experiments in a combustion facility are necessary to ascertain the ignition limits associated with such conditions.

## 9.1: Experimental Setup

The experiments to study the integrated design were conducted in an unheated supersonic wind tunnel, using a Mach 2.4 nozzle ($T_t$ = 300 K, $P_t$ = 379 kPa). An illustration of the plane where spectral measurements were made is shown in Figure 9.1a, along with a schematic of the relative location of the equipment in Figure 9.1b. Only ethylene was fed through the fuel injector, except for some preliminary experiments to ascertain the lifting effect of the aeroramp on the plasma jet where air was substituted. The torch feedstocks were methane, ethylene, nitrogen, and air, with heavy emphasis on the methane and nitrogen experiments. Regardless of the feedstock or arc gap being used, the torch chamber pressure was maintained at 345 kPa so that the results of one set of tests would be more comparable to another set.

(a) Illustration of Spectral Measurement Plane

(b) Tunnel Schematic Showing Injector,
Torch and Equipment Locations
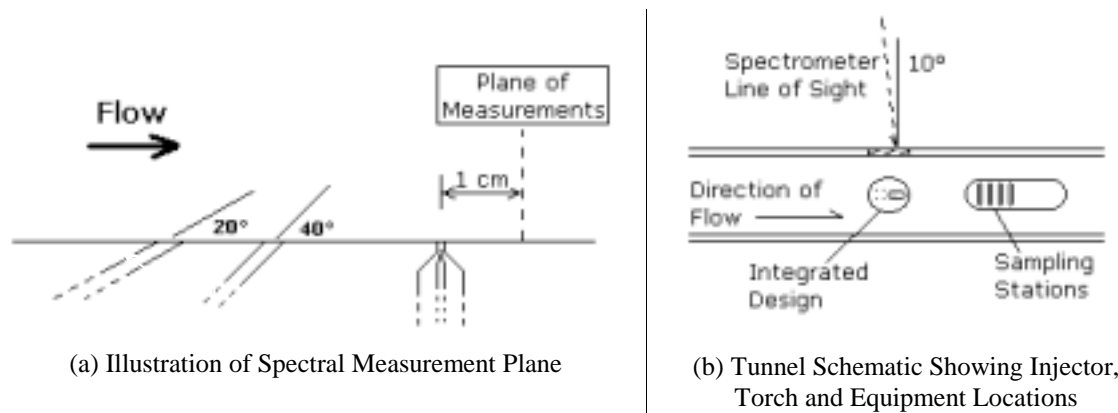
Figure 9.1: The Experimental Setup

Evaluation of the performance of the design was based on spectrographic measurements, total temperature measurements, and high-speed and filtered photography. Positioning stages were used to move the spectrometer line of sight so that a number of spectral samples of different spatial locations could be taken during a single run. These samples were primarily taken of the region 1 cm downstream of the torch exit, although other spatial locations were studied as well. In addition, the spectrometer line of sight was 10° off the normal direction, so that positions farther downstream could be observed through the small fused silica window. Further details of the setup for these experiments are included in Chapter 2.

### 9.2: Results and Discussion

The addition of an upstream aeroramp injector had a strong effect on the penetration distance of the plasma jet, particularly for higher momentum flux ratios. Figure 9.2 shows two black and white high-speed photographs taken of a nitrogen plasma jet (flow is from left to right) with air being fed through the upstream injector. This test was performed to determine the effects of injector momentum flux ratio on the penetration height of the plasma torch. For the photograph in Figure 9.2a, the air through the aeroramp injector was shut off to create a baseline condition from which to evaluate the lifting effect of the aeroramp. The plasma jet in the photograph is very bright and concentrated, with little penetration into the freestream. Increasing the mass flow rate of air through the injector caused the penetration height to increase, as shown in Figure 9.2b for an injector momentum flux ratio of 3.67. The increased penetration height is

attributed to the protective barrier provided by the aeroramp, and also the lifting effect induced by the counter-rotating vortices.



(a) $P_t$=900 W $q_t$=1.35, $q_{inj}$=0.00    (b) $P_t$=770 W, $q_t$=1.31 $q_{inj}$=3.67
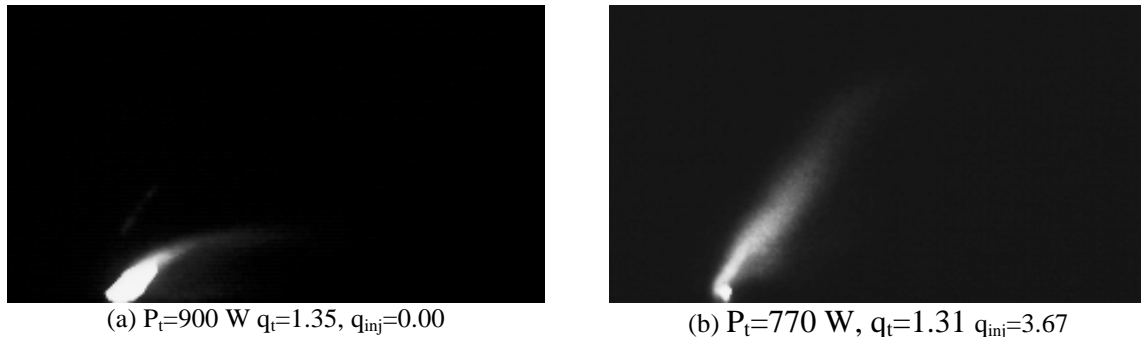
Figure 9.2: The Lifting Effect of an Upstream Aeroramp (scale: 5.1 cm x 2.8 cm)

The lifting experiments performed with nitrogen were repeated with methane, producing much the same results. Figure 9.3 shows several 35-mm photographs taken of the methane plasma jet, one without a filter and two with special filters to observe the qualitative distribution of CH and H radicals within the jet. Noteworthy among these photographs is the presence of a secondary jet structure, particularly evident in the CH photograph shown in Figure 9.3b. The hot jet core is clearly observed, with a secondary structure along the tunnel floor appearing to be trapped in the shear layer. This secondary jet was observed only rarely, and almost never as bright as in Figure 9.3b.



(a) No Filter (Exp. Time: 1 ms)    (b) CH Filter (Exp. Time: 1/125th)    (c) H Filter (Exp. Time: 1/125th)

Figure 9.3: Filtered Photographs Showing the Effect of Aeroramp Lifting on Plasma Species ($P_t$=2500 W, $q_t$=1.17, $q_{inj}$=3.00)

### 9.2.1: Methane-Ethylene Experiments

For experiments where ethylene was fed through the injector, and methane through the torch, a preliminary spectrographic analysis of the downstream products was necessary to identify the radicals present in the region of interest (i.e. 1 cm downstream of the plasma jet). The spectrogram in Figure 9.4 shows that only H, C, and $C_2$ radiate with any appreciable intensity in this region. Atomic hydrogen lines are common in most

hydrocarbon flames, but the presence of atomic carbon could be indicative of plasma, although this specie appears readily in hot flames with carbon-rich fuels as well. $C_2$ Swan bands are associated with hydrocarbon vapors passing through arcs with high current density, in addition to being quite common in most flames. Because of its intensity, the strong $C_2$ line at 516.5 nm was chosen as the measurement basis, particularly since no radicals associated with combustion, such as OH or $H_2O$, were present in sufficient concentration to produce strong signals. Measurements of the OH radical would be a natural choice for comparison of one test condition to another as it is associated with regions of intense combustion. However, the goal here was to evaluate how changes made in the fuel mass flowrate and torch power affected the distribution of various species downstream of the torch. So, in the absence of combustion-indicative species, the study of the distribution of $C_2$ should provide a good idea of trends associated with the design, such as penetration height or the effect of torch power on the fuel-plasma interaction rate. These trends associated with $C_2$ are expected to relate to combustion species if the experiments are repeated in a combustion facility. These concepts will be expanded in the following discussions.
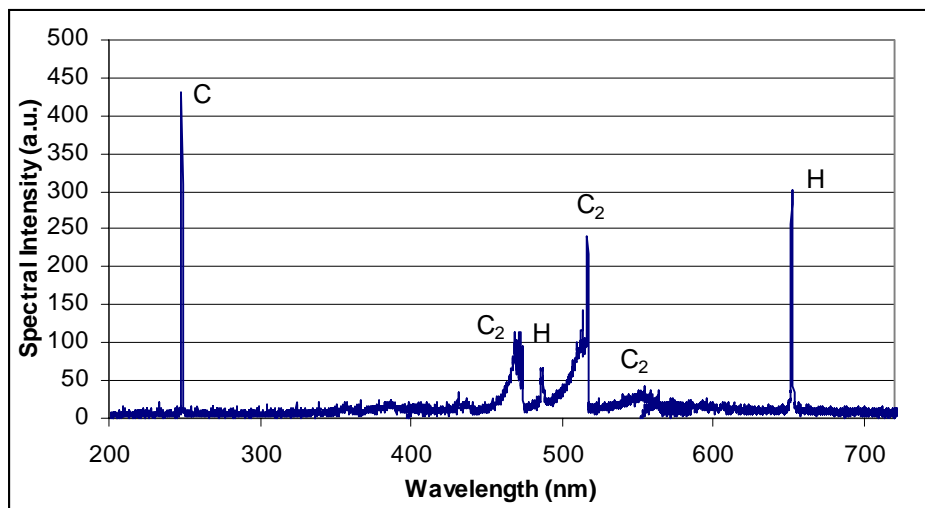


Figure 9.4: Spectrogram of Excited Ethylene/Methane Fragments by Methane Plasma Interaction (Taken 1 cm downstream of torch exit)

By traversing the spectrometer scope in the vertical direction, the distribution of $C_2$ emission intensity could be measured in a spanwise plane 1 cm downstream of the torch exit. The torch input power level was observed to have a noticeable effect on the

$C_2$ profiles intensity and to a lesser extent, the radical penetration height. Figure 9.5 shows five profiles for varying torch power and a constant injector momentum flux ratio of 3.0. As expected, the emission intensity increases with increasing power. However, by plotting the maxima of these profiles, an exponential trend was discovered between the torch input power and maximum observed intensity as shown in Figure 9.6. Earlier spectrographic studies of just the plasma jet in a crossflow (Chapter 6) showed only a linear increase in the intensity of the plasma jet with respect to the input power. Therefore, this exponential trend observed downstream of the plasma jet must be a function of the interaction of the plasma jet with surrounding hydrocarbon molecules. This trend is governed by Arrhenius kinetics, which state that the reaction rate of a particular reaction is a function of the concentration of the species participating in that reaction. One might argue that the plasma jet is simply interacting with the undissociated methane and not the ethylene from the fuel injector. Admittedly, a portion of the observed increase in emission is certainly from a higher concentration of dissociated methane. However, as will be shown later in the nitrogen-ethylene experiments, there is actually quite a bit of interaction between the plasma jet and fuel stream.
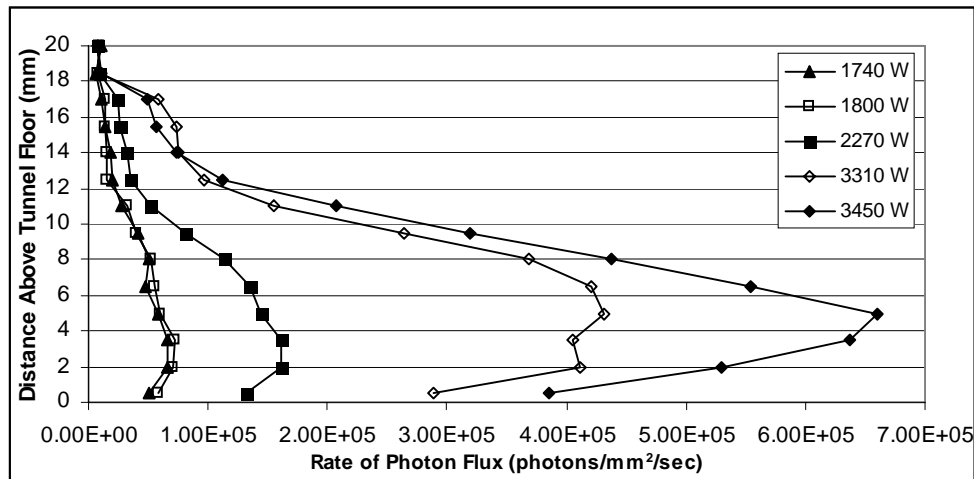


Figure 9.5: Changes of the Spectral Profiles of $C_2$ Line with Increasing Power for Methane Plasma (1 cm Downstream of Torch Exit, $q_t$=1.20, $q_{inj}$=3.00)

Figure 9.6 also contains the results from two other injector fuel flowrates, one with a momentum flux ratio of 1.5 and another with no fuel fed through the injector at all. Here, an unexpected trend was observed where the intensity of the $C_2$ line profiles decreased as the fuel flowrate was increased. This most certainly is a result of the fuel

acting as a heat sink, and perhaps should not be so surprising given the unheated condition of the tunnel. Ethylene has a much higher specific heat than air, so it would naturally extract a larger portion of the thermal energy from the plasma jet. In addition, this energy would be quickly convected away from the jet, having a reduced opportunity to dissociate fuel molecules. The case with no fuel injected through the aeroramp produces the highest $C_2$ profile intensities for powers above 2000 W. Injector momentum flux ratios of 1.5 and 3.0 produce lower intensities, respectively. However, around 1500-1700 W these trend lines merge. The reason for this is not clear, but indicates that at lower torch powers the $C_2$ line intensity is insensitive to the injector momentum flux ratio.
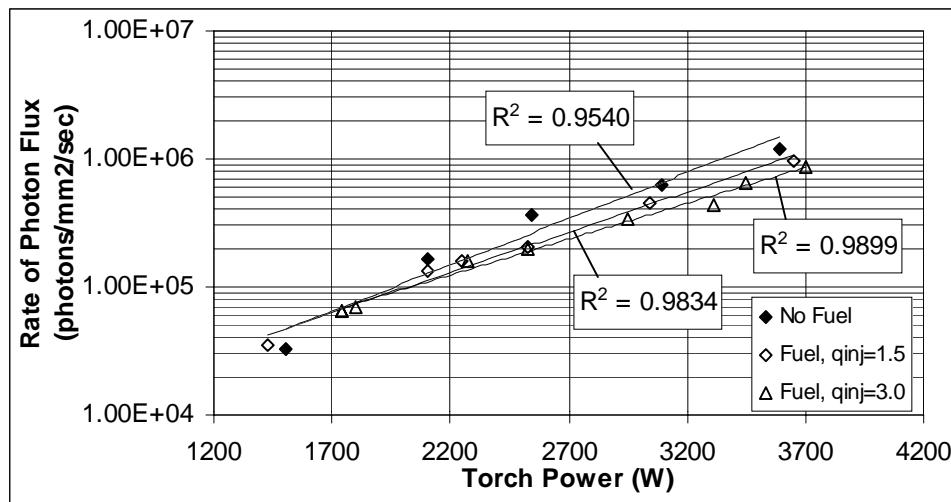


Figure 9.6: A Comparison of Fuel vs. No Fuel on the $C_2$ Line Intensity for Various Powers ($q_t$=1.20, 1 cm downstream of torch exit)

One might suggest that presenting just the spectral maxima of the profiles does not represent the profile as a whole. Plotted in Figure 9.7 are the spectral averages of the profiles presented in Figure 9.6 for a injector momentum flux ratio of 3.0. Clearly, the exponential trend is observed here as well, with just a slightly lower $R^2$ value, 0.9889 compared to 0.9899. Therefore, it can be convincingly stated that the presentation of just the spectral maxima is a good representation of trends for the entire profile.
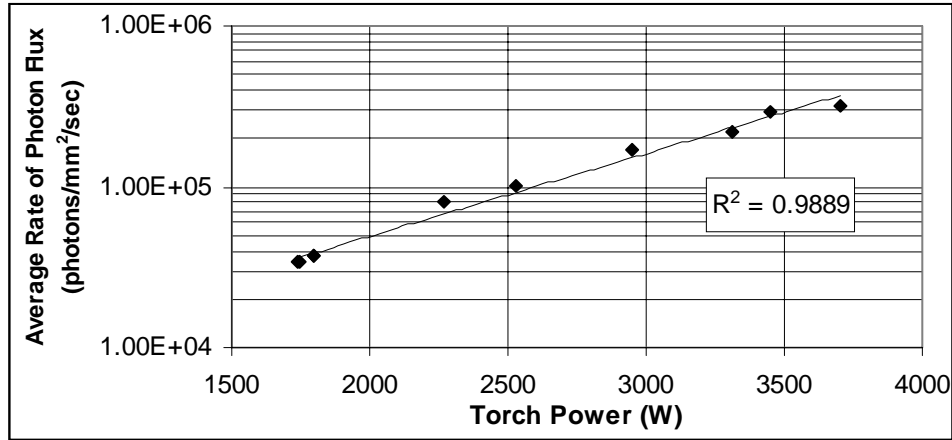
Figure 9.7: The Exponential Dependence of the Average $C_2$ Line Intensity on Torch Power ($q_t$=1.20, $q_{inj}$=3.00, 1 cm downstream of torch exit)

The effect of the injector mass flowrate was observed to have a similar effect on the $C_2$ profiles as the torch input power. Representative profiles for injector momentum flux ratios from 0 to 3.25 are show in Figure 9.8. As the mass flowrate of ethylene through the injector increases, the profiles become blunted and the penetration heights of the profile maxima increase. More importantly though, the spectral intensities of the profiles decrease as the fuel mass flowrate increases, attributed to the addition of thermal mass by the fuel. As was shown earlier, excitation by means of combustion plays a very minor role in the spectral intensities for these conditions, and so the addition of fuel would not be expected to increase the intensity of the downstream products. This is similar to the effect of increasing the feedstock flowrate through the torch, which was observed to cause a decrease in the spectral intensity of the plasma jet (Chapter 7). In the present case, the thermal quenching of the plasma jet by the added fuel exhibits the same result. As the fuel flowrate through the injector is increased, the thermal energy imparted to the fuel remains the same since the source is constant. In fact, the energy transfer may even increase because of the higher fuel concentration and the fact that the specific heat of ethylene is much higher than air, indicative of a higher rate of heat transfer. However, the added fuel in turn lowers the bulk temperature of the downstream products and hence, reduces the concentration and spectral intensity of excited species. Nevertheless, the trend shown here for unheated conditions does not imply that in a high-enthalpy tunnel the added fuel would quench the flame. Rather, these trends simply show that the addition of fuel serves as a heat sink in cold conditions.
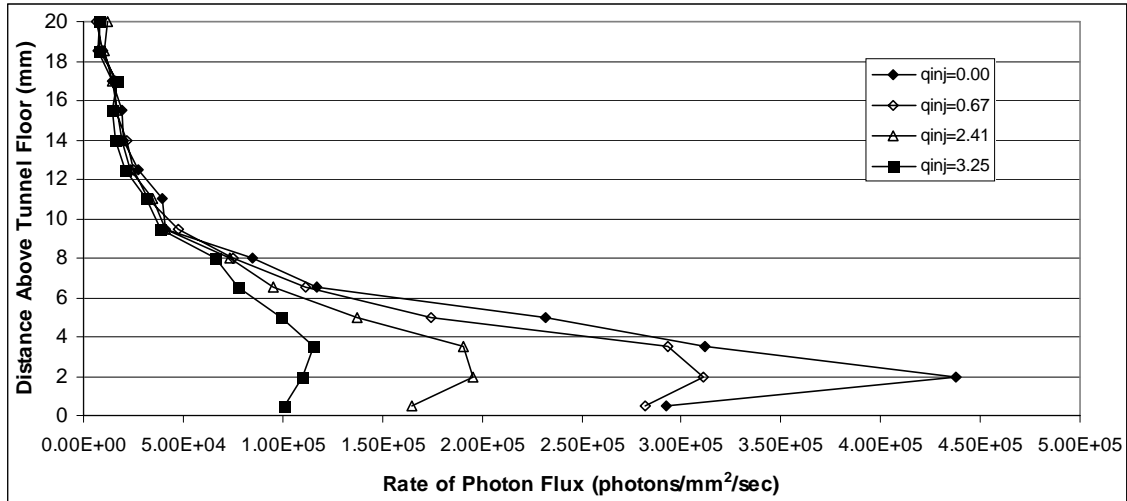
Figure 9.8: $C_2$ Line Profiles for 2500 W and Various Injector Momentum Flux Ratios for Methane Plasma ($q_t$=1.20, 1 cm downstream of torch)

To support this argument, experiments were performed to study the maximum observed $C_2$ intensity for a wide range of fuel flowrates. The results are plotted in Figure 9.9 and demonstrate that the addition of fuel serves to act as a heat sink to the plasma jet. Here the spectral maxima of a number of $C_2$ profiles are plotted versus the injector momentum flux ratio. Even through the data scatter, the trend is clear that as the momentum flux ratio is increased, the spectral intensity of the $C_2$ profiles levels off. The trend line shown in the plot is a second order polynomial, producing a decent correlation. The addition of fuel, particularly above injector momentum flux ratios above 1.5, show little decrease in the spectral maxima. This trend is actually quite similar to the one observed in Figure 9.6 where the profile intensity was insensitive to the amount of fuel addition at lower powers. These concepts are inherently linked and suggest that, because of the chemically reactive nature of the plasma jet, a plasma jet will produce at least a minimum concentration of excited species regardless of the local fuel concentration. The importance of this actually lies in the fact that the plasma jet cannot be extinguished merely through the addition of fuel.
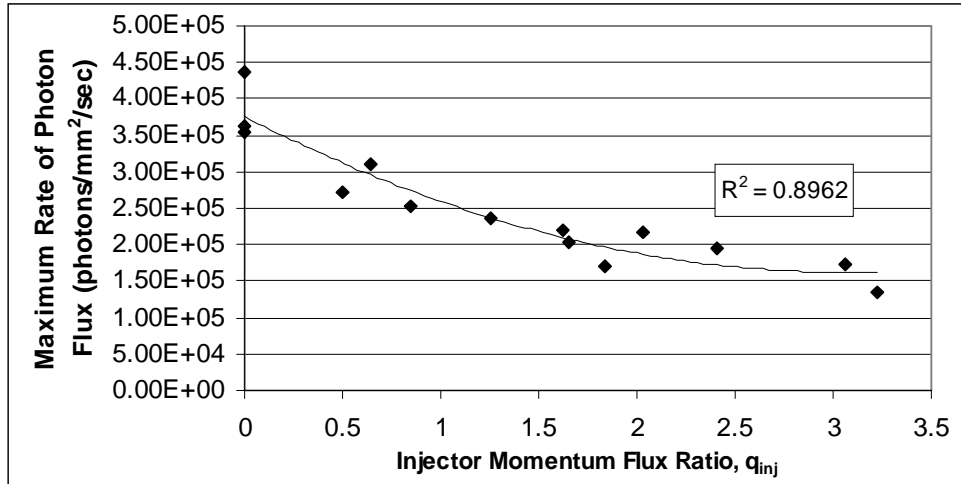
Figure 9.9: The Effect of Increasing the Fuel Mass Flowrate on the Intensity of $C_2$ Line
($q_t$=1.20, $P_t$=2500 W, 1 cm downstream of torch)

Figure 9.10 presents the $C_2$ profile maxima at different spatial locations from the torch for a single set of operating conditions. In Figure 9.10, the spectral intensities of $C_2$ and hydrogen increase rapidly closer to the torch exit. However, it was also desired to take spectral measurements outside of the plasma region. The point to make here is that the data taken at the 1 cm downstream position were taken at the most ideal location, a position where the spectral intensity has dropped off significantly, to such a point that it can be assumed to be outside of the plasma jet, but not so low that spectral measurements become difficult to obtain.
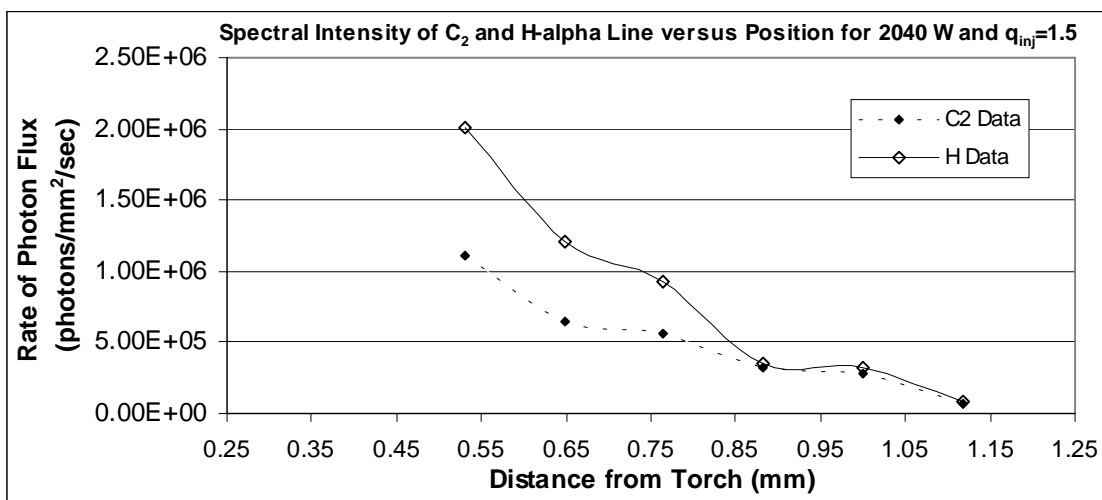


Figure 9.10: Distribution of the Maximum $C_2$ Line Intensity versus Distance from Torch
Exit ($P_t$=2040 W, $q_t$=1.20, $q_{inj}$=1.50)

Filtered photography was useful for providing a detailed qualitative look at the plasma jet and its intensity and profiles in different spectral regions. Figure 9.11 shows four such photographs for 2000 W, where flow is from left to right. As expected, the $C_2$ molecule produces the brightest and largest profile, matching earlier trends in the quiescent environment (Figure 7.6) regarding the propagation distance and spectral intensity of the various species. Expectedly, the crossflow causes the plasma jet to lean over. The oddly shaped, intense region in the $H_2$ photograph is a bead of molten molybdenum and is not to be confused with the plasma jet core.



(a) $C_2$ Filter          (b) CH Filter

(c) H Filter          (d) $H_2$ Filter

(e) Scale
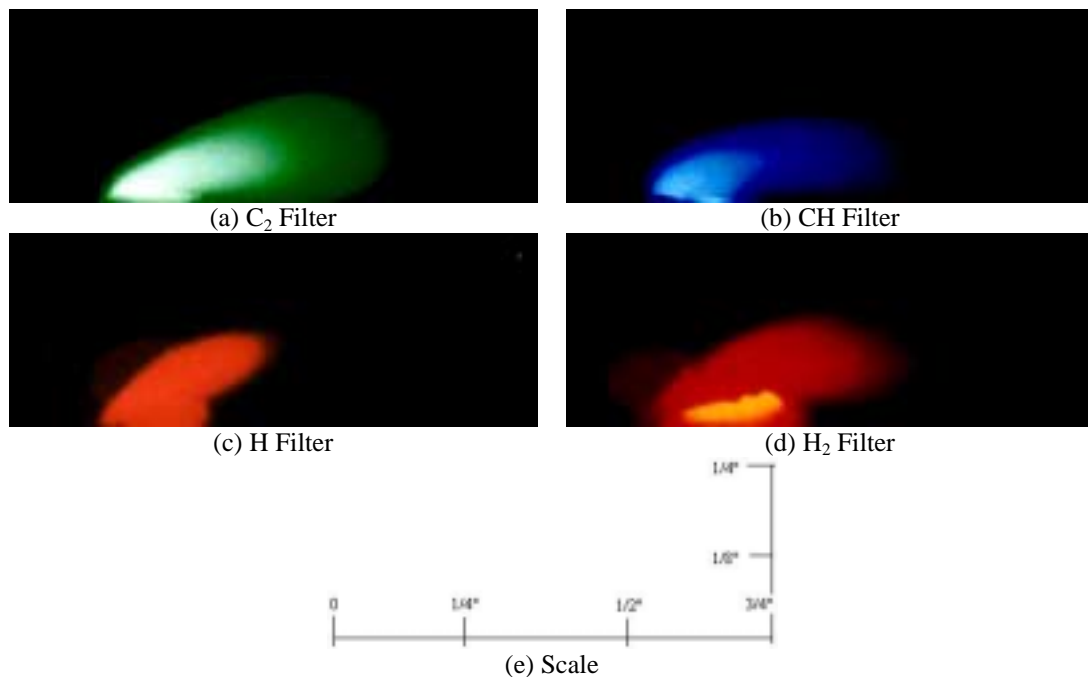
Figure 9.11: Filtered Photographs of Methane Plasma Jet for 2000 W
($q_t$=1.20, $q_{inj}$=1.50, Exp. time: $1/125^{th}$ sec)

To qualitatively support the trends associated with the spectrographic work, filtered photographic techniques were used to observe the effects of torch power and fuel mass flowrate on the shape of the plasma jet. A CH filter was used for these studies since spectrographic work showed that excited CH was contained almost wholly within the plasma jet (refer to Figures 7.5 and 9.4), and would allow for easy identification of the plasma jet boundary. In Figure 9.12, five CH photographs are presented for powers ranging from 1430 to 3650 W. Expectedly, as the power supplied to the torch increases,

both the intensity and size of the jet increase, but the added power does not seem to appreciably affect the penetration height of the plasma jet.



(a) 1430 W    (b) 2100 W    (c) 2250 W

(d) 3040 W    (e) 3650 W    (f) Scale
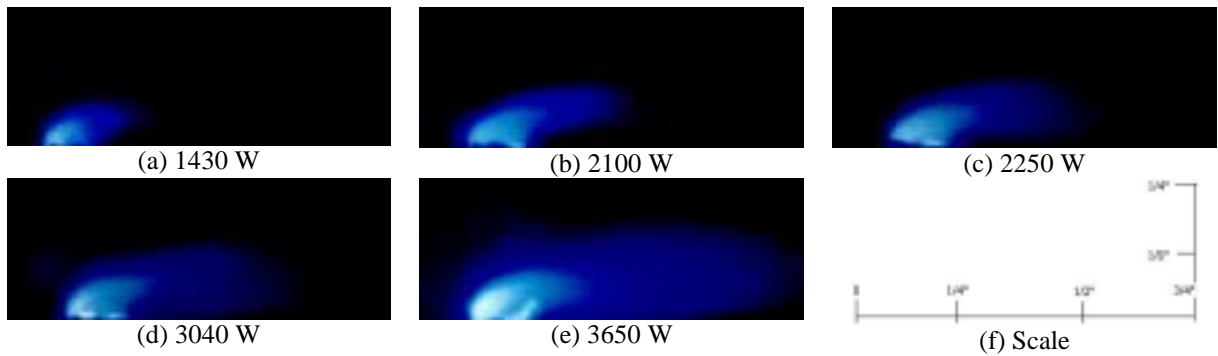
Figure 9.12: CH Profile Variations with Increasing Power
($q_t$=1.20, $q_{inj}$=1.50, Exp. time: 1/125th sec)

The penetration height of the plasma jet was influenced more by the mass flowrate of fuel fed through the injector, as demonstrated earlier in Figures 9.2 and 9.3, than increases in the torch power. In this case, a wider range of injector momentum flux ratios was tested to determine exactly when the lifting effect of the aeroramp becomes significant. As shown in Figure 9.13, aeroramp injector momentum flux ratios below 1.6 produce no noticeable effect on the shape or penetration height of the plasma jet. However, between injector momentum flux ratios of 1.25 and 1.62, the plasma jet is clearly observed to lift off of the floor, penetrating further into the crossflow for increasing momentum flux ratios. Not only is this trend observable in the surrounding dim regions of the jet, but the core seems to be affected as well.



(a) $q_{inj}$=0.00    (b) $q_{inj}$=0.85    (c) $q_{inj}$=1.25

(d) $q_{inj}$=1.62    (e) $q_{inj}$=2.41    (f) $q_{inj}$=3.06
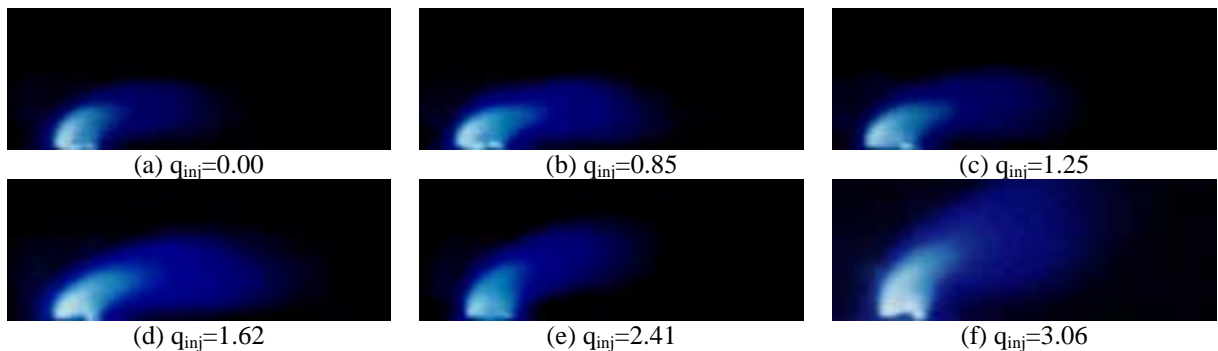
Figure 9.13: CH Profile Variations with Increasing Injector Mass Flowrate
($P_t$=2500 W, $q_t$=1.20, Exp. time: 1/125th sec)

Total temperature measurements were used to ascertain how the thermal energy contained within the plasma jet was being mixed into the aeroramp plumes. A 2D total temperature ratio profile for a torch power of 2000 W and an injector momentum flux ratio of 1.5 is shown in Figure 9.14. The symmetric structure of the total temperature plot indicates that the thermal energy imparted by the plasma jet is being evenly mixed into both sides of the injector plumes. In addition, the mushroom-like appearance of the plume indicates, as with the CH photographs, that the excited species are being lifted off the floor of the tunnel and into the crossflow. Earlier experiments with a plasma torch and no upstream injector produced profiles with higher total temperature ratios (due to the absence of fuel acting as a heat sink), but had lower penetration, indicating that increased penetration and mixing occurs due to the addition of an upstream aeroramp.
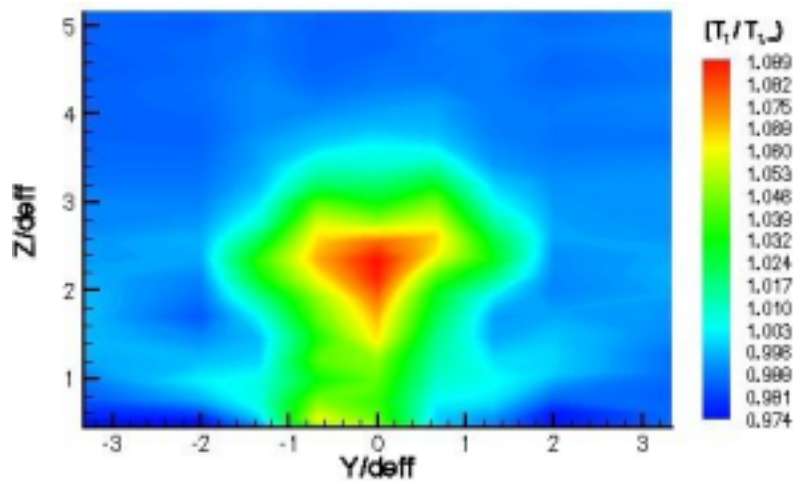


Figure 9.14: 2D Temperature Profile of Methane Plume at 2000 W
($q_t$=1.20, $q_{inj}$=1.50, $x/d_{eq}$=31.6)

### 9.2.2: Nitrogen-Ethylene Experiments

Unlike the methane-ethylene experiments, the species produced in the nitrogen-ethylene experiments could easily be attributed to the nitrogen plasma, the ethylene fuel, or a product of the two. A typical spectrogram taken 1 cm downstream of the plasma jet is shown in Figure 9.15. The excited exhaust contains excited $C_2$, as with the methane, and $N_2$ from the torch. However, the exhaust also contains a very strong presence of CN, a product of a hydrocarbon vapor being introduced to active nitrogen, indicating an appreciable amount of plasma-fuel interaction. The absence of excited hydrogen and

carbon atoms indicates that this region contains little, if any, plasma. This may also explain the absence of excited CH molecules, since they are primarily associated with the plasma jet and are short-lived. For the experiments involving nitrogen feedstocks, the intensity of CN emission was chosen as the measurement basis since CN is a direct indicator of fuel-plasma interaction.
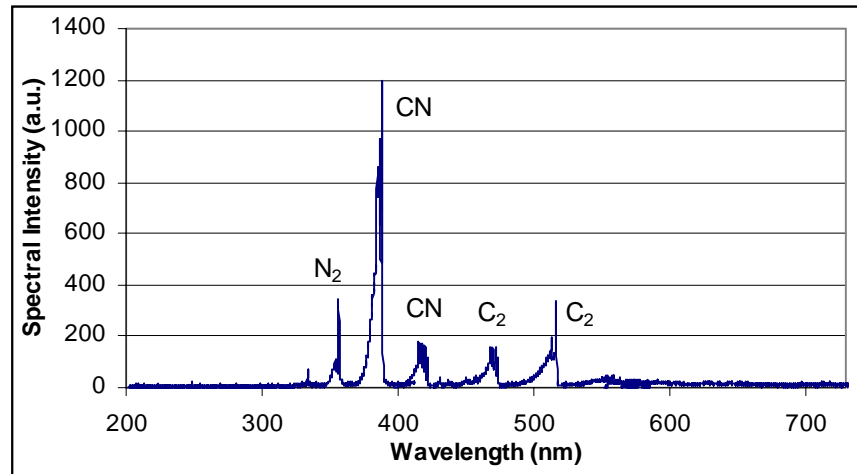


Figure 9.15: A Spectrogram of Excited Ethylene and Nitrogen Species by Interaction with a Nitrogen Plasma Jet

One opportunity afforded by using a nitrogen feedstock, which was not possible with the methane tests, was the ability to test how increasing arc gaps affected the various results. In actuality, it was a necessity to increase the arc gap, since for the standard gap of 0.178 mm it was difficult to produce torch powers above 2000 W. The relatively low specific heat of nitrogen, when compared to methane and heavier hydrocarbons, makes it challenging to extract a large amount of energy from the arc, particularly for short arc lengths. This study was conducted to determine if the slope of the exponential trend was at all dependent upon the length of the arc gap. The results of spectrographic surveys for two separate arc gaps are shown in Figure 9.16. As expected, the CN profile intensities are much higher for the longer arc gap than for the shorter arc gap, but the slopes of the trend lines do not seem to be a function of the arc gap as shown in Figure 9.17. In addition, the penetration heights of the CN profile maxima do not seem to be affected by the length of the arc gap.
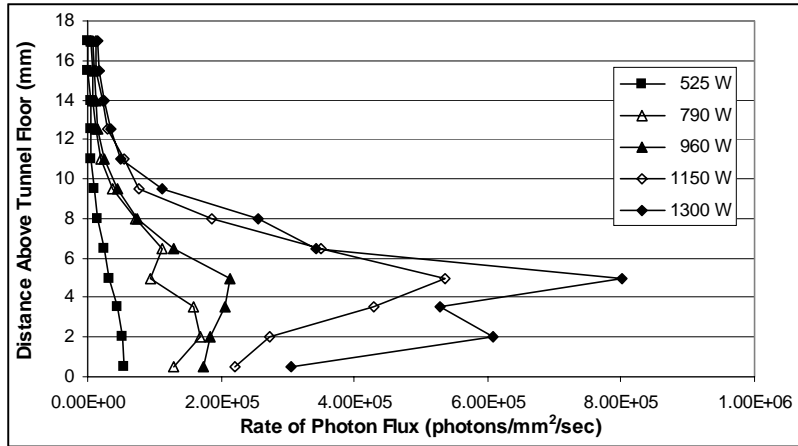
(a) Arc Gap of 0.178 mm
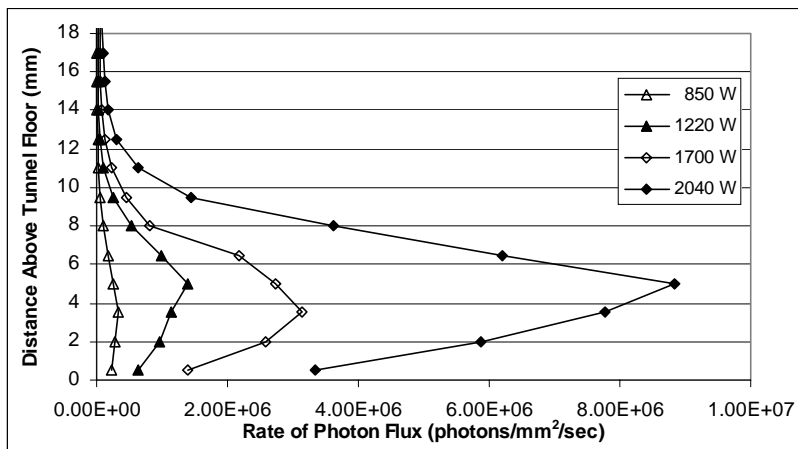


(b) Arc Gap of 0.267 mm

Figure 9.16: Profiles Showing the Effect of Arc Gap on CN Distribution for Nitrogen Plasma (1 cm Downstream of torch exit, $q_t$=1.2, $q_{inj}$=1.5, CN Line at 388.3 nm)

By plotting the maxima of the profiles presented in Figure 9.16, it is evident that the spectral intensity represented by the trend line exhibits an exponential dependence on torch input power. These effects are shown in Figure 9.17. In addition, it seems that increasing the arc gap serves to increase the efficiency of the torch as higher concentrations of excited species are produced for a given power. This indicates that the constrictor thermal entry length has not yet been reached for the given current. Furthermore, because CN is a product produced only through fuel-plasma interaction, the exponential trend observed in Figure 9.18 can now convincingly be attributed to the amount of fuel with which the plasma jet chemically reacts. Also, this dependence is a

function of power, indicating that increasing the power supplied to the torch creates an exponential return.
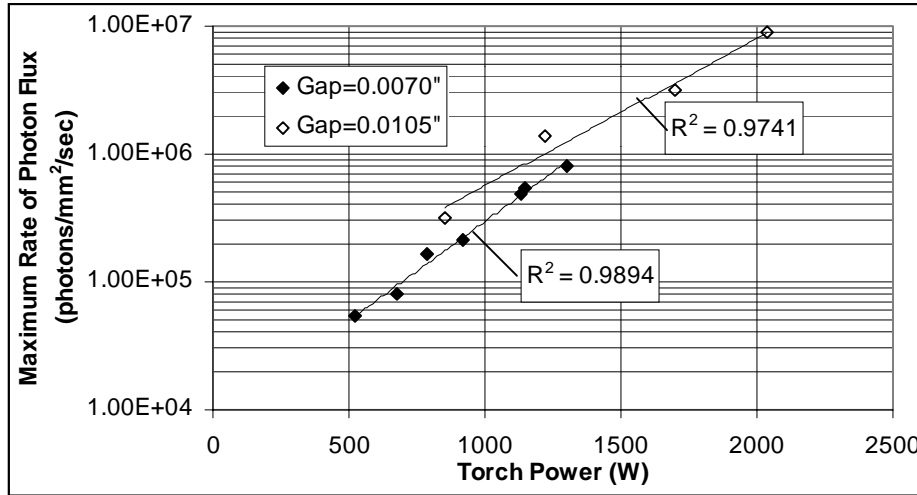


Figure 9.17: CN Line Maxima for Two Arc Gaps
($q_t$=1.2, $q_{inj}$=1.5, 1 cm downstream of torch, CN Line at 388.3 nm)

As stated earlier, for a given power increase, the plasma jet experiences a linear increase in intensity, corresponding to a linear increase in excited specie concentration. Increasing the specie concentration within the plasma jet appears to cause an exponential increase in reaction rates associated with fuel-plasma interactions. It is important to note that although these trends are observed in a cold tunnel, the trends are expected to carry over to a combustion facility, so that with a very small increase in electrical power a large increase in combustion efficiency might be realized.
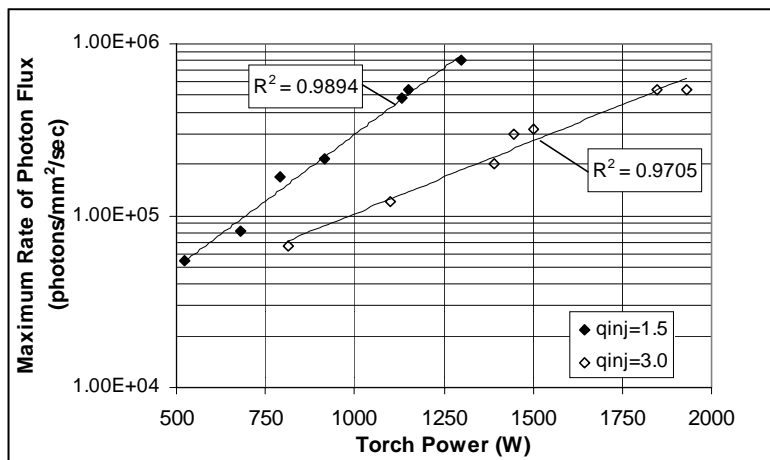


Figure 9.18: A Comparison of Fuel Mass Flowrate Effects on CN Line Intensity
($q_t$=1.2, Arc Gap=0.178 mm, CN Line at 388.3 nm)

Increasing the mass flowrate of fuel through the injector had the same effect with the nitrogen experiments as with the methane, that is, increasing the fuel mass flowrate decreases the emission intensity of the downstream products. Figure 9.18 shows the results of two of these tests. The trend lines approach each other at low powers, as in the methane experiments. Again, the reason for this is not known, but the figure shows that at powers below about 500 W the emission intensity of downstream products appears to be independent of the injector fuel mass flowrate.

In addition to the spectral data taken 1 cm downstream of the torch exit, spectral data at other locations around the plasma torch exit were taken to construct intensity profiles of excited species near the torch exit. Because the ethylene injectant and nitrogen feedstock contained no common atoms, it was easy to separate the source of the radical in question. Consequently, by understanding the nature and source of particular radicals, identification of the plasma jet boundary could be made. These profiles are shown in Figure 9.19, where the torch exit is located at x = 0 mm. The CN and $C_2$ profiles look quite similar, with their maxima occurring directly above the torch exit where the plasma jet is most intense. The drop-off in intensity of these species is gradual as they travel downstream and mix with the cooler surrounding gases. The lack of sustainable combustion under these conditions prevents the formation of new excited molecules once the fuel has left the plasma region. Evidence of excited CN and $C_2$ is present in front of the plasma jet as well, formed in the recirculation region between the jet centerline and bow shock. Figure 20c shows a profile for excited $N_2$ and presents a very good idea of the shape and size of the plasma jet. Furthermore, the profiles of atomic carbon and hydrogen, shown in Figures 20d and 20e, indicate the most intense regions of fuel-plasma interaction. Here, through intense thermal and chemical interaction with the plasma jet, some of the fuel molecules have been dissociated into their atomic components. The maxima of atomic carbon and hydrogen occur just upstream of the plasma torch exit in a subsonic separation region. These atomic species reach the ground state or recombine before they propagate more than 6 or 7 mm from the plasma torch exit. This demonstrates that the spectral measurements made 1 cm

downstream of the torch exit for nitrogen-ethylene experiments can be assumed to be outside of the plasma region.



(a) N$_2$ Profile (357.7 nm)

(b) C$_2$ Profile (516.5 nm)

(c) CN Profile (388.3 nm)

(d) C Profile (247.8 nm)

(e) H Profile (656.3 nm)

Conditions:
$q_t$=1.24
$q_{inj}$=1.50
$P_t$=2040 W
Arc Gap= 0.267 mm
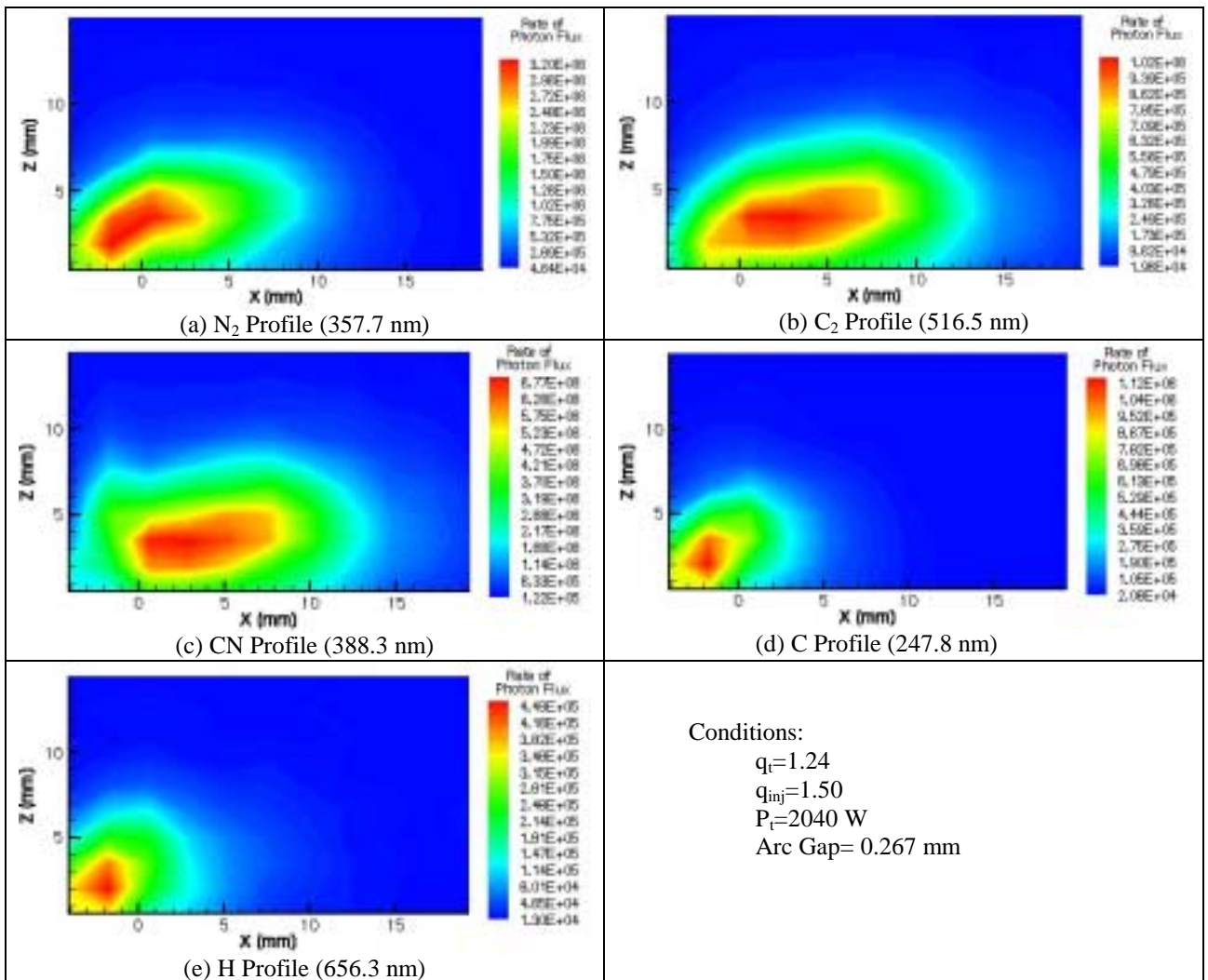
Figure 9.19: Radical Profiles Near Torch Exit

Filtered photographic techniques were used to aid in the interpretation of the trends identified in the spectrographic work presented in Figure 9.19. The photographs of particular interest are those presented for the hydrocarbon species associated with the ethylene, mainly, CN, H, H$_2$, and C$_2$. An unfiltered photograph is shown in Figure 9.20a as comparison. It is interesting to note that the CN, C$_2$, and H profiles shown in Figure 9.20 qualitatively match quite well with the spectrographic profiles presented in Figure 9.19. The C$_2$ and CN plumes both originate at the plasma jet exit and exhibit strongly luminous cores. Excited hydrogen produces a much smaller profile than the other

species, supporting the trends observed in the spectrographic work. The remaining pictures, (g) and (h), were taken through spectral filters associated with $H_2$ and OH. However, these species were not observed to radiate strongly in the spectrographic study, so it would be incorrect to label the pictures as being associated with those species. More likely, the luminous regions observed at these wavelengths are a result of the broadband emission from the plasma jet, part of which radiates within the spectral range of the filters. As a whole, the pictures provide a good qualitative look at the distributions of various species within the jet, and the emission characteristics of the region at different wavelengths.



| (a) No Filter (Auto exposure, $q_{inj}$=1.56) | (e) H Filter (656 nm, 1/500th, $q_{inj}$=1.65) |
| (b) CN Filter (388 nm, 1/30th, $q_{inj}$=1.62) | (f) CH Filter (431 nm, 1/500th, $q_{inj}$=1.43) |
| (c) CN Filter (410 nm, 1/500th, $q_{inj}$=1.60) | (g) (600 nm, 1/1000th, $q_{inj}$=1.53) |
| (d) $C_2$ Filter (516 nm, 1/500th, $q_{inj}$=1.62) | (h) (306 nm, 1 sec, $q_{inj}$=1.56) |
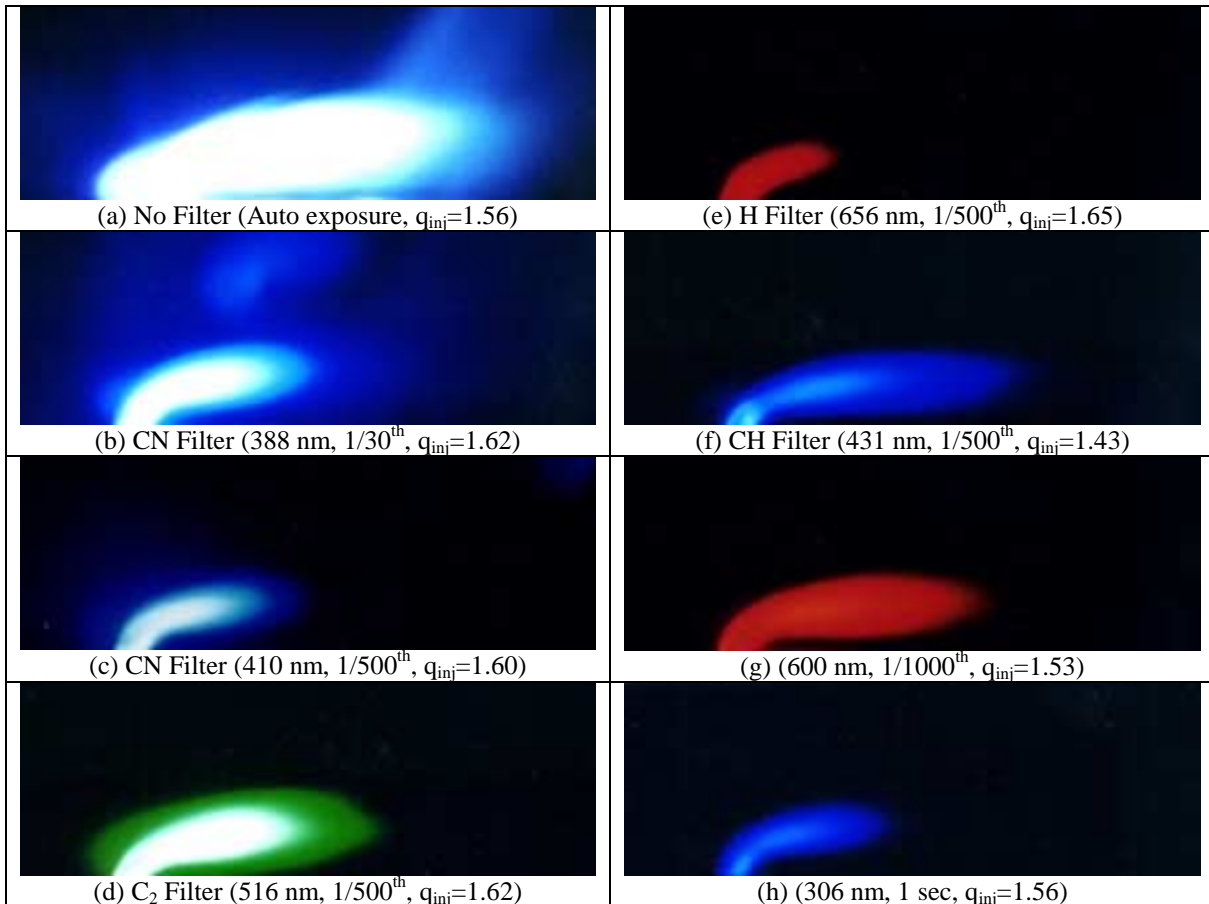
Figure 9.20: Filtered Photographs for Nitrogen-Ethylene at 2000 W
($q_t$=1.24, scale: 5.1 cm x 1.7 cm)

The effect of power on the plume size and shape was studied using the CH filter, as with the methane experiments, the results of which are shown in Figure 9.21. Comparison to the methane results in Figure 9.12 reveals important differences. The

most noteworthy is the effect of power on the plume intensity. The methane results showed a rather modest increase in CH intensity for powers ranging from 1400 to 3600 W, whereas here changes in power of as little as 300 or 400 W produce a much larger gain in the plume luminosity. In the nitrogen-ethylene experiments, the production of CH is attributed solely to the ethylene and not to the torch feedstock. Therefore, the CH photographs demonstrate that the rate of reaction between the plasma jet and fuel increases exponentially with torch power, as evidenced by the plume luminosity and supported by the trends observed in Figures 9.17 and 9.18. In addition, the penetration height of the luminous region also increases slightly with torch power, indicating reactions between the fuel and plasma are occurring farther out into the crossflow.



(a) CH Filter (1/30$^{th}$, 1990 W, $q_{inj}$=1.58)　　　(c) CH Filter (1/30$^{th}$, 2770 W, $q_{inj}$=1.57)

(b) CH Filter (1/30$^{th}$, 2400 W, $q_{inj}$=1.58)　　　(d) CH Filter (1/30$^{th}$, 3020 W, $q_{inj}$=1.34)
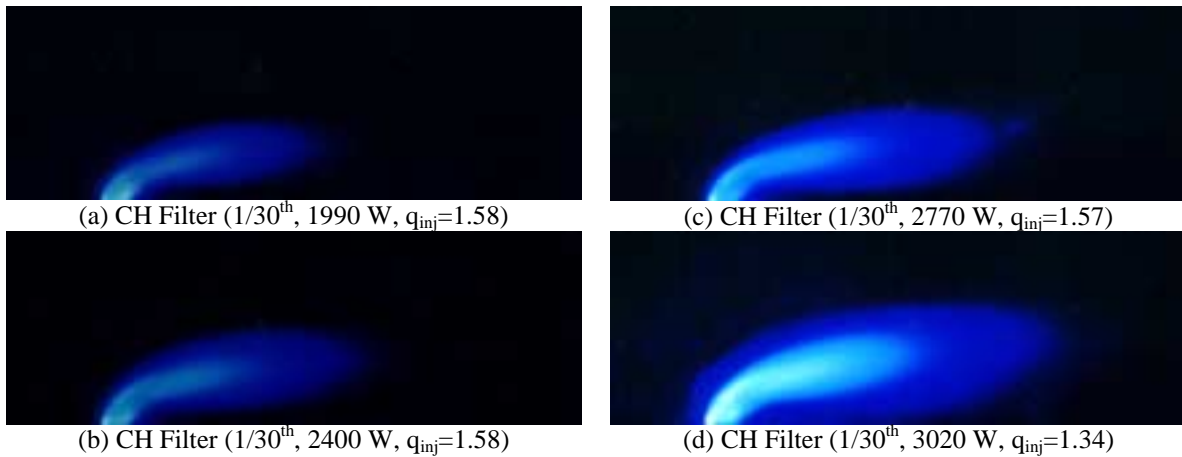
Figure 9.21: Photographs Demonstrating the Effect of Increasing Power on the CH Profile ($q_t$=1.24, scale: 5.1 cm x 1.7 cm)

To capture phenomena that the slower optical techniques could not detect, an unfiltered high-speed camera was used. The most interesting of the photographs collected during the study are shown in Figure 9.22, where flow is from right to left and ethylene fuel is being injected upstream of the nitrogen plasma jet. Figure 9.22a shows a well-defined plasma jet with radiating species being swept downstream. However, the important aspect in this photograph is the identifiable attachment point of these species on the floor, just downstream of the plasma jet. This region is a separation zone, identified in earlier oil flow visualization studies, and provides an anchoring point for a flame. Since this phenomenon was previously unobserved with the plasma torch studies, these species are thought to be excited products of the cracked ethylene molecules, rather

than excited nitrogen species being swept off the jet. Figure 9.22b supports this idea, which shows the plasma jet at the trough of the voltage cycle. Due to the oscillation of the power supplies, the plasma jet will not appear in the photograph for a single point in the voltage cycle. Despite the absence of the plasma jet, it is clear that these excited species are still present, and longer-lived than the nitrogen species contained in the plasma. The importance of this photograph suggests that a pulsed plasma jet may be just as effective as a DC jet for maintaining combustion in a supersonic flow.



(a) Separation Zone Influences    (b) Excited Species in "Trough" of Plasma Jet Cycle
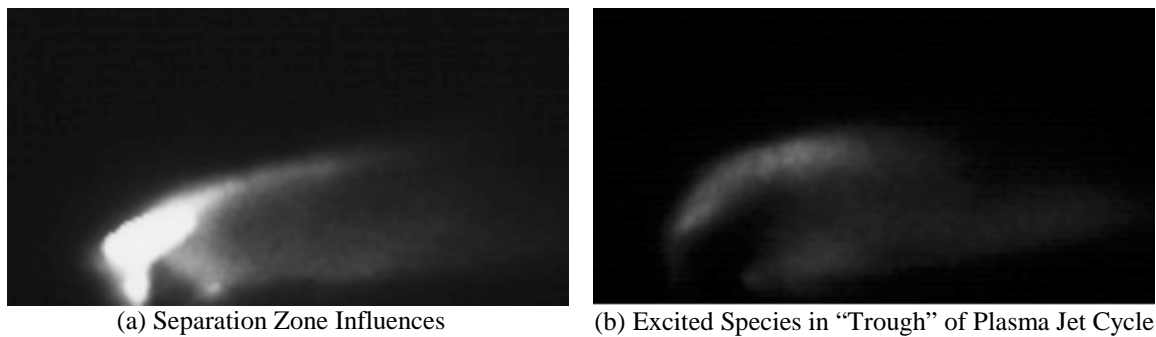
Figure 9.22: Evidence of Fuel Interaction with Nitrogen Plasma Jet
($P_t$=700 W, $q_t$=1.27, $q_{inj}$=3.35)

To complement the spectral measurements of the fuel-plasma products, total temperature measurements were made to study how the thermal energy produced by the torch was mixing into the injector plumes. The total temperature profile shown in Figure 9.23 looks very similar to the profile made during the methane experiments under the same conditions, but close examination reveals a distinct difference. Although the penetration height of the plume core is roughly equivalent to the methane profile, the core is shifted slightly to the right, indicating the thermal energy is not being evenly mixed between the two injector plume cores. In addition, the maximum total temperature measured here is slightly higher than measured with the methane feedstock, 1.10 versus 1.09. The specific heat of nitrogen is lower than methane, indicating it should produce a lower value of total temperature since it will absorb less energy from the arc for a given arc length. However, the higher measured value could be attributed to the increased arc gap used to make this profile (higher efficiency), poorer mixing (although this is not likely considering the aeroramp is the main mixing device), or from a small amount of combustion causing some heat release. Regardless of the cause, the important aspect of

the plot is that the lifting effect is still certainly present as evidenced by the mushroom shape of the profile.
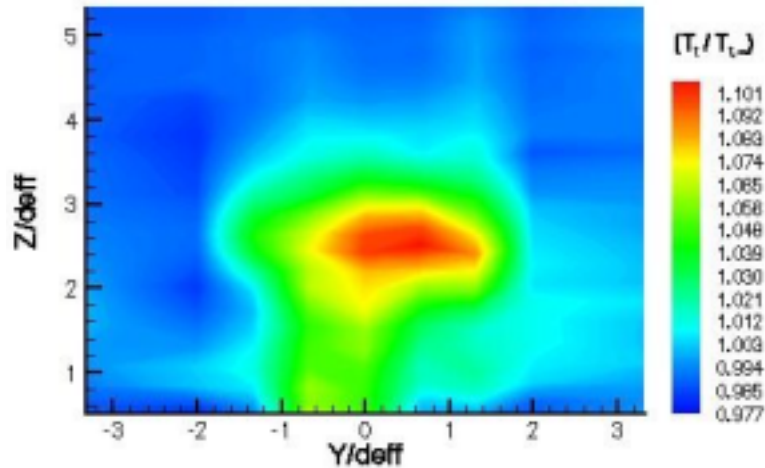


Figure 9.23: 2D Temperature Profile for Nitrogen Plume at 2000 W
($q_t$=1.24. $q_{inj}$=1.50, Arc Gap=0.267 mm, $x/d_{eq}$=31.6)

## 9.2.3: Ethylene-Ethylene Experiments

Experiments using ethylene as a feedstock were conducted to determine how the use of heavier hydrocarbons affects the ignition potential of the plasma torch. To date, the use of ethylene as a torch feedstock has been largely uninvestigated, with almost all studies concentrating on air, nitrogen and hydrogen-argon feedstocks. One notable exception is a paper by Harrison et al. (1971) where the potential of using ethylene is discussed. It is well known that the ignition potential of hydrocarbon feedstocks lies in the production of hydrogen atoms, and it is thought that for a larger molecule these hydrogen atoms may be more easily stripped. This is related to the dissociation bond energy, which is the enthalpy (per mole) required to break a given bond between two atoms in a molecule. The bonds with smaller bond energies are, by definition, easier to break. Furthermore, the energy required to break a bond is a function of the atoms associated with the bond, which determine the bond length and difference in electronegativity. Consequently, not all C-H bonds require the same energy to break. Breaking the first C-H bond in a methane molecule requires 435 kJ/kmol, whereas only 411 kJ/kmol are required to break the first C-H bond in ethylene. Consequently, this is the same phenomenon that makes it difficult to burn methane. In addition, given the specific heats of the two gases, ethylene will absorb more energy from the arc. The

combination of these two thermodynamic principles suggests that for a constant mass flowrate and power, an ethylene feedstock should produce a larger number of hydrogen atoms. Unfortunately, due to the difficulty of operating the plasma torch with ethylene, only a limited amount of runs were possible to verify if this was the case. However, even from the limited data collected, important trends were observed that hold relevance for supersonic combustion applications.

Figure 9.24 shows four $C_2$ profiles made with ethylene as both the injectant and feedstock. As experienced with the earlier methane and nitrogen experiments, the addition of fuel appears to quench the radicals as the fuel absorbs thermal energy from the jet. In addition, there appears to be an exponential increase in the profile maxima as power increases. Furthermore, the penetration height does not seem to be affected by power. These results show little difference from earlier results with methane. However, comparison with the profile maxima for methane show that the $C_2$ profile intensities presented here are much higher.
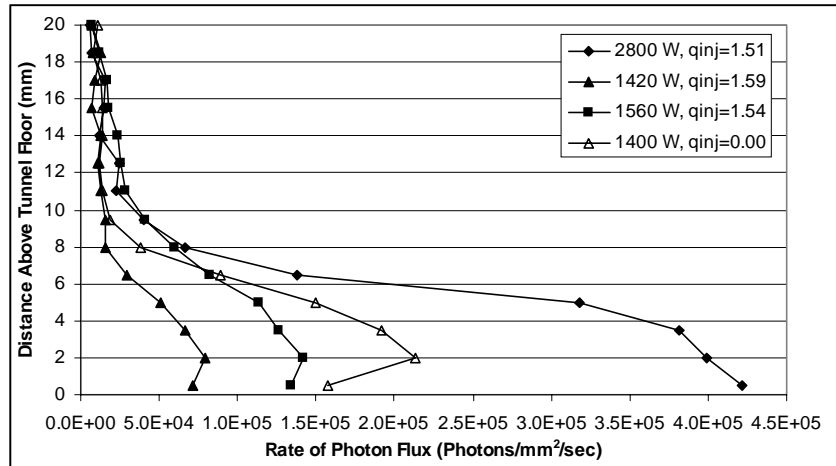


Figure 9.24: Changes of the Spectral Profiles of $C_2$ Line with Increasing Power for Ethylene Plasma ($C_2$ line at 516.5 nm, 1 cm downstream of torch exit, $q_t$=1.25)

Figure 9.25 shows a comparison of $C_2$ profile maxima taken 1 cm downstream of the torch exit for both methane and ethylene feedstocks. Two trends are immediately recognized from the plot. First, the $C_2$ maxima for the ethylene experiments are an average of 100% higher than the corresponding methane experiments for the same power. Second, the trend lines are both exponential, and parallel to each other. On the most

fundamental level, these results demonstrate that an ethylene feedstock produces higher concentrations of excited $C_2$ molecules than a methane feedstock. If the trend continues, heavier hydrocarbons would be expected to perform even better. However, since both the feedstock and fuel are ethylene it is difficult to ascertain whether the increase in emission is due to the addition of $C_2$ molecules from the feedstock, or an increased rate of reaction with the fuel. It is expected that the trend observed in Figure 9.25 cannot solely be attributed to the addition of excited $C_2$ from the feedstock, since it well known that hydrogen atoms are more easily stripped off a more complex hydrocarbon molecule. Furthermore, it is believed that the excited $C_2$ molecules observed downstream of the torch are a direct result of the higher concentration of hydrogen atoms produced by the ethylene torch feedstock. If such were the case, this would mean that heavier hydrocarbons, as opposed to lighter hydrocarbons, would make superior feedstock igniters based on their chemical nature allowing the production of hydrogen atoms at a lower energy cost. However, the issue of an increased rate of electrode erosion associated with the heavier hydrocarbon feedstocks must also be addressed.
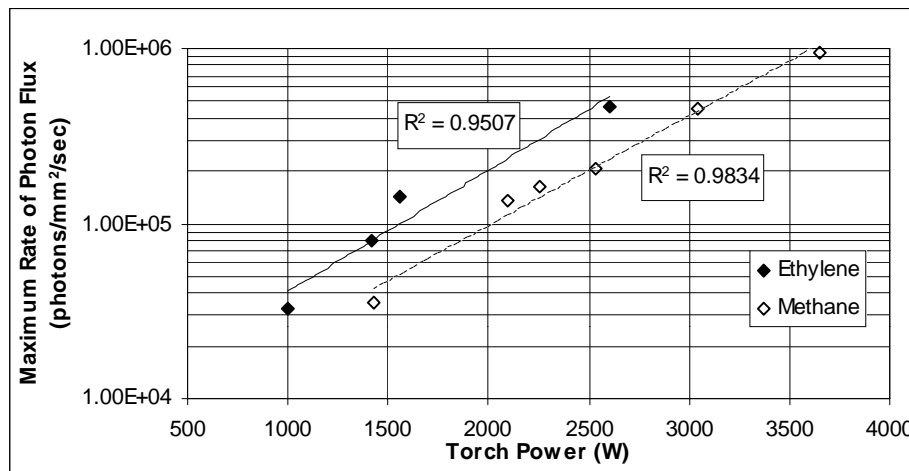


Figure 9.25: The Exponential Dependence of $C_2$ Line Intensity on Torch Power and Feedstock (1 cm downstream of torch exit, $q_t$=1.25, $q_{inj}$=1.55)

### 9.2.4: Air-Ethylene Experiments

Earlier experiments with nitrogen and air have produced mixed results to which feedstock is a better ignition source (Kimura, 1981; Sato, 1996). The ignition potential of nitrogen is based on its ability to produce oxygen atoms through the Zeldovich

mechanisms, which then go on to react with the fuel. From a torch efficiency standpoint, it is theorized that pure oxygen would make the best feedstock, simply based on its bond energy in comparison to nitrogen (498 kJ/kmol versus 945 kJ/kmol). Unfortunately, testing with pure oxygen produces safety hazards that labs are not generally not equipped to handle, so tests with air are usually substituted. Air, being composed of primarily two different gases is difficult to operate with for extended periods of time, a result of the different molecular chemistries and specific heats of nitrogen and oxygen. Gallimore (1998) noted these difficulties with methane and argon, both of which are relatively stable feedstocks, but when mixed produced unstable performance. Although the present experiments with air demonstrated excellent ignition potential, it is expected that a pure oxygen feedstock would produce even more impressive results.

Like ethylene, the experiments with air were limited due to the severe erosion problem experienced with air plasma. Copper anodes were used to maximize the operational lifetime, but even with these only a handful of runs were possible. However, even from these limited runs, it was noticed that the results were quite different than for those of the previous torch feedstocks. The test cell was much brighter during the runs, and in several instances at powers near 3000 W, a definite flame was observed extending 10 to 15 centimeters down the tunnel. This flame was whitish in color near the torch exit and almost as intense as the plasma jet itself. Away from the plasma jet, the flame had the characteristic dull blue color of a burning hydrocarbon. The presence of burning ethylene in this case is undeniable, even though this conclusion is based only on physical observation. However, it cannot be understated that the presence of a flame in the cold Mach 2.4 crossflow is absolutely remarkable, and must be due to the production of oxygen atoms. Undoubtedly, repetition of these experiments in a high-enthalpy tunnel would produce very promising results.

The spectrogram shown in Figure 9.26 was used to identify the species present within the flame 1 cm downstream of the torch exit. The most intense peaks in the region are attributed to CN radiating at 388 nm. The strong Swan bands of $C_2$ are also present at 516.5 nm. There are some additional peaks as well, identifying CH at 431 nm, and HCO around 330 nm. The peaks of HCO in this region are known as Vaidya's hydrocarbon flame bands, and occur in the inner cone of hydrocarbons, but are especially

strong in low-temperature flames of ethylene and air. The lack of strong OH bands near 306 nm is a result of the low temperature environment within the tunnel.
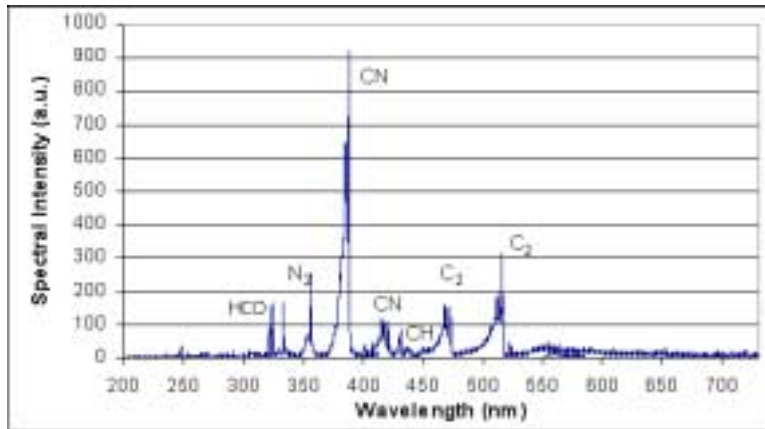


Figure 9.26: A Spectrogram of Excited Ethylene and Air Species by Interaction with an Air Plasma Jet

Only two runs of the six attempted produced spectral profiles of importance, one at 1650 W and another at 3050 W, and are shown in Figure 9.27. The 1650-W $C_2$ profile exhibits the characteristic shape observed with other feedstocks, with the intensity dropping off 7-10 mm above the floor. However, the 3050-W profile has a completely different contour. The spectral intensity of the $C_2$ molecule does not diminish significantly, even up to 2 cm above the tunnel floor. This matches well with observations made during the high-power runs when a large, intense flame was produced. Also noteworthy is the height above the floor at which the $C_2$ molecules radiate. The emission presented here occurs only 1 cm downstream of the torch in a Mach 2.4 crossflow. This demonstrates that the combustion enhancing radicals produced by the torch have an almost immediate effect well out into the crossflow, due in part to the lifting effect of the aeroramp, but also certainly to the reactive nature of the species produced.
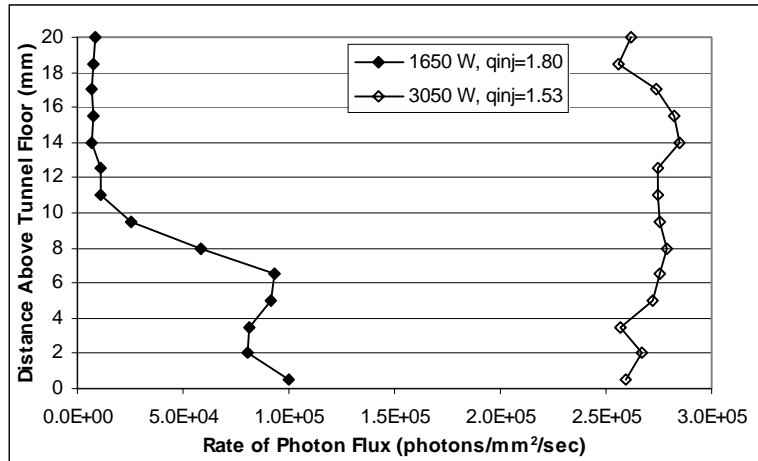
Figure 9.27: Changes of the Spectral Profiles of $C_2$ Line Intensity with Increasing Power for Air Plasma ($C_2$ line at 516.5 nm, 1 cm downstream of torch exit, $q_t$=1.25)

To support the spectrographic work, several filtered photographs were taken of the test cell during the air-ethylene runs. Two photographs taken through CH and $C_2$ filters are shown in Figure 9.28. Comparison to other photographs of this type reveal that the plumes presented here are much longer. It is irrefutable that the $C_2$ profile shown in Figure 9.28a is evidence of combustion, since the plasma certainly could not exist far enough downstream to account for the emission at the tail end of the emitting region. The curved region near the right side of the photograph is caused by the window edge, which the flame actually extends several centimeters beyond. In addition, the plumes are also dimmer, requiring a longer integration time. This is characteristic of a flame, as they are less intense than plasma. These purely qualitative results are exciting, in that they suggest air may be an excellent candidate to use as a feedstock in this design if the erosion problem can be effectively dealt with.
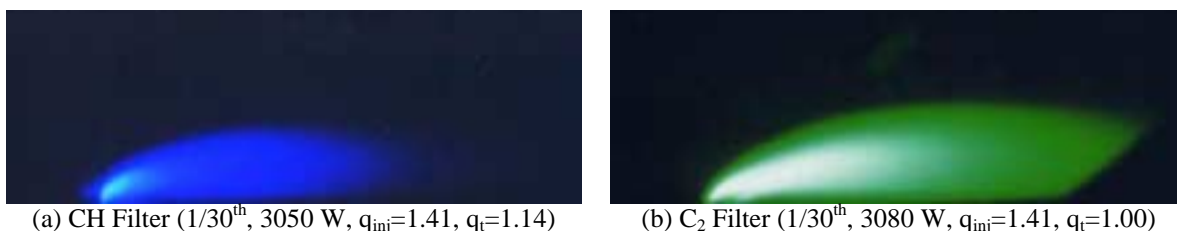


(a) CH Filter (1/30th, 3050 W, $q_{inj}$=1.41, $q_t$=1.14)      (b) $C_2$ Filter (1/30th, 3080 W, $q_{inj}$=1.41, $q_t$=1.00)
Figure 9.28: A Comparison of CH and $C_2$ Profiles for Air-Ethylene Tests
(Scale: 5.1 cm x 1.7 cm)

Finally, total temperature sampling was used to produce the 2D temperature profile shown in Figure 9.29. The profile is perfectly symmetric because only two sets of data (3 probes per set) were collected with which to produce the profile, one set at the centerline and one 1.59 mm to the left of the centerline. These data sets were then mirrored to produce the other half of the profile. The penetration characteristics of the plume are similar to those of the other feedstocks, with a majority of the thermal energy provided by the torch being lifted off of the tunnel floor. The maximum total temperature ratio is 1.32, much higher than for the other feedstocks, but the power here is also higher so it cannot be concluded whether the higher total temperature value is due in part to combustion, or is wholly a result of the thermal energy provided by the torch. It is expected that at least a small percentage of the total temperature rise is due to combustion, since the presence of combustion was observed during the tests.
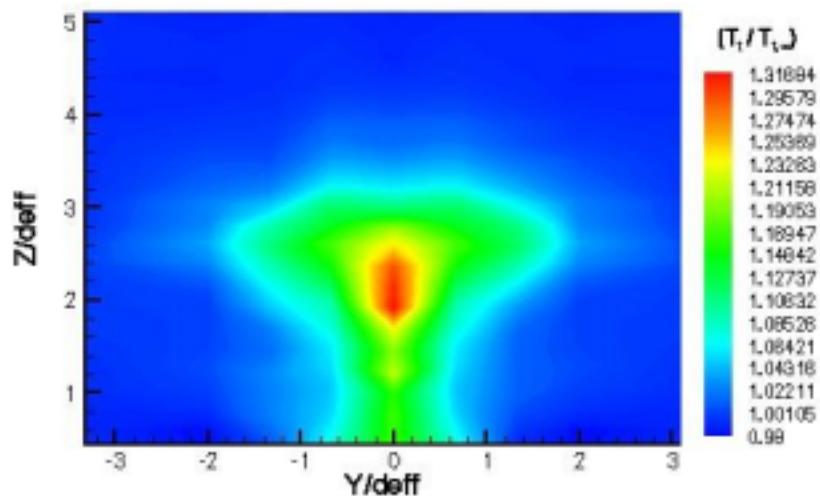


Figure 9.29: A 2D Temperature Profile for Air Plume at 3000 W
($q_t$=1.14, $q_{inj}$=1.53, $x/d_{eq}$=31.6)

### 9.2.5: Electrode Emission

Throughout this dissertation, it has been stated that electrode particles may play a role in combustion applications as micro-flameholders. However, none of the earlier observations of electrode emission were made while fuel was being injected upstream of the torch. The photographs presented in Figure 9.30 were made under such conditions during the nitrogen-ethylene experiments. Each photograph shows evidence of electrode emission to one degree or another, but the photograph in Figure 9.30d is particularly

interesting, not because it has just a single electrode particle in the photograph, but because there is a faint luminous trail behind the particle. This trail is highlighted by an arrow and is the result of heat transfer from the particle to the surrounding gases. This luminous trail is thought to be evidence of a very limited amount of combustion. It is also known that the addition of small particles of various metals enhances the combustion process. Work by Tepper and Kaledin (2001) demonstrated that the addition of nano-aluminum particles could be used as a combustion accelerant. The development of a torch with a consumable cathode, or one designed to operate on a feedstock seeded with these types of particles, could achieve much higher ignition potential than the standard torches of today.



| (a) 1500 W, $q_{inj}$=3.42 | (c) 900 W, $q_{inj}$=1.42 |
| (b) 3660 W, $q_{inj}$=3.67 | (d) 1500 W, $q_{inj}$=3.42 |
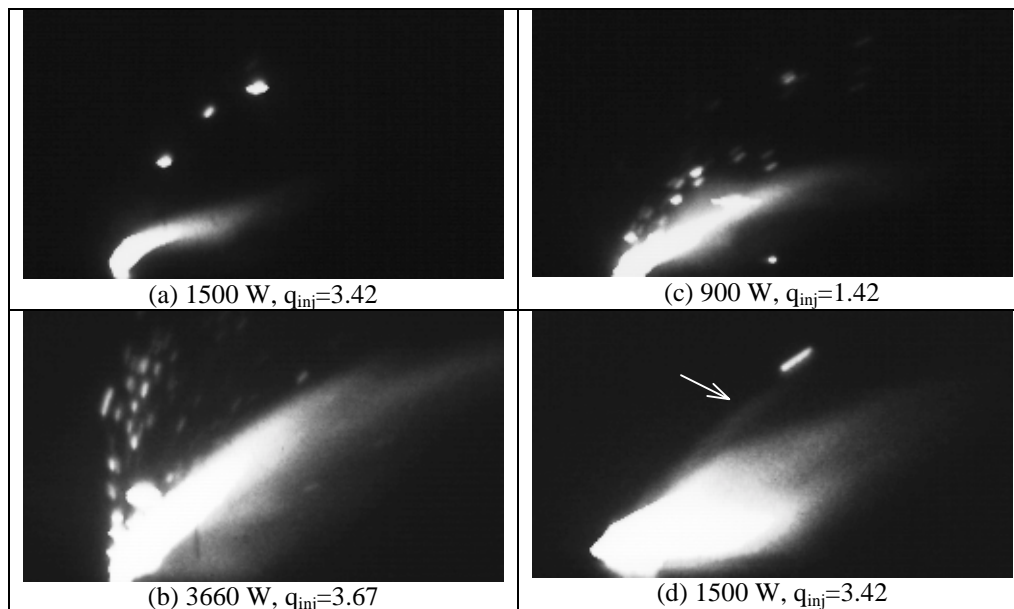
Figure 9.30: High-speed Photographs Showing Particle Injection

## 9.3: Conclusions

The experiments presented here were part of an extensive research program designed to investigate the integration of an aeroramp injector and plasma torch, and to discover any possible synergistic effects of the combination. The goals of the research were to discover to what extent the aeroramp injector assists the propagation of radicals contained within the plasma jet by means of the counter-rotating vortices induced by the injector. In addition, variations in the fuel flowrate through the injector and the power of the torch were made to ascertain how various conditions changed the performance of the design.

Spectral measurements, filtered photography, and total temperature sampling were used to provide a full-picture view of the local, near-downstream, and far-downstream phenomena associated with the design. The main observations made from the research are:

- The aeroramp injector significantly increases the penetration height of excited species contained within the plasma jet, particularly for injector momentum flux ratios above 1.5.
- Increasing the torch power was observed to cause an exponential increase in the emission intensity of downstream products for all feedstocks. This was attributed to an increase in the chemical reaction rate between the fuel and plasma.
- For the cold-flow conditions of the supersonic tunnel, the addition of fuel served to act as a heat sink and reduce the intensity of excited species.
- It was discovered that the decrease in spectral intensity due to the reduction of power or increase in the fuel flowrate leveled off, indicating that the plasma torch cannot be quenched by the mere addition of fuel.
- Downstream total temperature measurements showed that the thermal energy contained within the plasma jet was being distributed nearly equally between the two plumes produced by the aeroramp.
- At high powers, air was observed to produce a highly luminous flame plume extending about 10 cm down the test section. This was attributed to the presence of atomic oxygen in the plasma.

The practical application of these results can be realized in any supersonic combustor design that employs the use of a plasma igniter and a lifting mechanism to increase the penetration height of the radicals into the crossflow. Perhaps the most important aspect of this work is the identification of combustion-enhancing trends associated with the use of different feedstocks. Ethylene was identified as being superior to methane as a combustion-enhancing feedstock based on a higher production of hydrogen atoms for a given power input. Furthermore, air was observed to produce a

flame even within the cold-flow conditions of the tunnel. The practical application of these results indicates that if a plasma torch is to be used as an ignition source, very careful consideration must be made not only at what power to operate the torch, but also which feedstock would be most useful.